Nanocomposite Hydrogel with Temperature Response for Capacitive Energy Storage

Jose Garcia-Torres,[a,b,c,*] Samuele Colombi,[b,d] Ikraan Mahamed,[a] Dioulde Sylla,[e] Marc Arnau,[b,d] Jordi Sans,[b,d] Maria-Pau Ginebra,[a,b,f] and Carlos Alemán[b,d,f,*]

[a] *Biomaterials, Biomechanics and Tissue Engineering Group, Department of Materials Science and Engineering and Research Center for Biomedical Engineering, Universitat Politècnica de Catalunya (UPC), 08019, Barcelona, Spain*

[b] *Barcelona Research Center in Multiscale Science and Engineering, Universitat Politècnica de Catalunya, 08019 Barcelona, Spain*

[c] *Institut de Recerca Sant Joan de Déu, 08034 Barcelona, Spain*

[d] *Departament d'Enginyeria Química, EEBE, Universitat Politècnica de Catalunya, C/ Eduard Maristany, 10-14, 08019, Barcelona, Spain*

[e] *IREC-Catalonia Institute for Energy Research, 08930, Sant Adrià de Besòs, Spain*

[f] *Institute for Bioengineering of Catalonia (IBEC), Barcelona Institute of Science and Technology (BIST), Baldiri Reixac 10-12, 08028 Barcelona Spain*

[*] jose.manuel.garcia-torres@upc.edu and carlos.aleman@upc.edu

ABSTRACT

Functional hydrogels are 3D polymeric networks with potential applicability in the field of wearable electronics. However, hydrogels are often used to develop devices with only one functionality. In this work, a multifunctional hydrogel consisting on poly(3,4-ethylenedioxythiophene) (PEDOT), alginate (Alg), carbon nanoparticles (CNP) and manganese oxide has been manufactured for devices that can simultaneously store energy (supercapacitor) and sense temperature. The Alg and PEDOT interpenetration allows obtaining a flexible and electrically conductive hydrogel with open and interconnected porous structure. The incorporation of CNP improves the electrical conductivity and confers synergies with the manganese oxide, which provide energy storage capability. Furthermore, the resistance of the hydrogel varies linearly with the temperature, this behavior being observed consistently and without hysteresis throughout consecutive heating and cooling cycles. Thus, the PEDOT/Alg/CNP/MnO_2 hydrogel shows good capacitance (42 mF cm^{-2}), capacitance retention (87 %), and good temperature sensitivity (-1.05% $°C^{-1}$).

INTRODUCTION

Among hydrogels, which are three-dimensional network structures able to imbibe large amounts of water, conducting hydrogels (CHs) deserve consideration due their charge (ionic and/or electronic) transport properties. CHs are excellent candidates for the fabrication of flexible electronics owing to their good conductivity, adjustable mechanical properties (*i.e.* stretchability, compressibility, and elasticity), multiple stimuli-responsive properties, conformability and biocompatibility.[1,2] Within this context, CHs have emerged as promising candidates for manufacturing flexible bioelectronics devices for diagnosis (*e.g.* biosensors) and therapeutics (*e.g.* drug-delivery systems), playing vital roles in health monitoring, soft robotics, regenerative medicine or artificial intelligence (*e.g.* electronic skin).[1,3-8] More recently, CHs have been successfully used for manufacturing flexible energy storage devices (*e.g.* batteries and supercapacitors for energy conversion)[8-10] and solar water evaporator equipment for seawater desalination and wastewater purification[11] due to other interesting advantages, such as large surface area, porous microstructure and easy tenability.

Among the different types of existing CHs, those prepared by incorporating carbon based materials such as carbon nanotubes (CNTs), carbon black (CB), and graphene into insulating hydrogels have received special attention because of the outstanding properties of the resulting nanocomposites hydrogels.[12,13] For example, carbon-based CHs are widely used for sensing applications and electrical double-layer electrochemical supercapacitors (EDLCs) due to their excellent mechanical and electrical properties as well as high surface area.[14,15] Other nanoparticles (NPs)-based CHs are those containing transition metal oxide hydrogels. These nanocomposite CHs, which utilize reversible redox reactions at the electrolyte-electrode interface, are used in pseudo-supercapacitors because of their high capacitance.[16,17] One limitation of these single functional hydrogels, and at the same time a challenge, is that they can only match a single demand at a time, limiting their applicability.

CHs prepared by mixing poly(3,4-ethylenedioxythiophene) (PEDOT) and alginate (Alg) have received special attention because of their multi-responsive behavior.[18] PEDOT is a commercially available organic conducting polymer (CP) with outstanding conductive and electrochemical responses (*i.e.* high conductivity and fast redox response), high processability, mechanical robustness, exhibits improved electrical conductivity, and good biocompatibility.[19-21] On the other hand, Alg is a natural, biodegradable, biocompatible, biostable, and hydrophilic polysaccharide extracted from brown algae.[18,22] Interpenetrated hydrogels obtained by combining PEDOT and Alg, hereafter named PEDOT/Alg, simultaneously exhibit the properties of the two systems, as for example conductivity, piezoelectricity, biocompatibility, self-healing properties, and both chemical and thermoelectric responsiveness.[18] Because of this, PEDOT/Alg CHs have been proposed for soft (bio)electronics as self-healable pressure sensors,[23] drug delivery system,[24,25] biosensor (when loaded with gold nanoparticles for signal amplification),[26] remotely transportable electronic devices (when loaded with magnetite nanoparticles),[27] among others.[18]

This work goes one step further by designing a new multifunctional PEDOT/Alg hydrogel that incorporates carbon nanoparticles (CNP) and a metal oxide, manganese oxide (MnO_2), for its simultaneous use as flexible supercapacitor and temperature sensor. Each material plays a relevant role within the hydrogel to get this multifunctionality. While Alg confers mechanical stability as it can be easily cross-linked by bivalent cations, PEDOT and CNP generate an electrically conductive path across the hydrogel, and MnO_2 has a high energy storage capacity (theoretical capacitance: 1370 F g^{-1}).[28]

METHODS

The materials and characterization methods are described in the Electronic Supporting Information (ESI), this section reporting only the preparation methods.

The hydrogels -PEDOT/Alg, PEDOT/Alg/CNP and PEDOT/Alg/CNP/MnO_2- were prepared by mold casting. The utilization of a mold is essential to control the shape and dimension of the hydrogels in a reproducible manner. The process can be summarized as follows. First, equal volumes of a commercial PEDOT:PSS suspension (1.3 wt.%) and a sodium alginate solution (3.9 wt.%) were homogeneously mixed using a speed mixer (3500 rpm, 5 min). The mixture was injected into the mold cavity and introduced into a 0.2 M $CaCl_2$ solution to crosslink the polymeric chains and get the hydrogel. To prepare the PEDOT/Alg/CNP hydrogel, CNP were added to the PEDOT/Alg dispersion to get a final content of 30 wt.%. Finally, the PEDOT/Alg/CNP hydrogels were modified by chemical reduction of $KMnO_4$ with ethanol to get PEDOT/Alg/CNP/MnO_2. Hydrogels were immersed in 5 mL of ethanol (EtOH) and subsequently 3 mL of 0.1 M $KMnO_4$ solution were added. Different times, ranging from 5 min to 60 min, were waited to have different amounts of manganese oxide. Hydrogels were thoroughly washed in deionized water.

RESULTS AND DISCUSSION

Preparation of the hydrogels

PEDOT/Alg/CNP/MnO_2 hydrogels were synthesized as shown in Figure 1. First, a homogenized dispersion of PEDOT, Alg and CNP was poured into a mold in which the ITO-coated PET sheet was previously placed. After that, the mold was immersed in a $CaCl_2$ solution for Alg crosslinking. In order to incorporate the MnO_2 to the formed hydrogels, gelled samples were immersed in EtOH and $KMnO_4$ was added. Hydrogels were kept for different times (5, 15, 30 and 60 min) in the reaction medium to modify the MnO_2 content coming from the reduction of permanganate. Figure 1 includes photographs of as prepared PEDOT/Alg/CNP and PEDOT/Alg/CNP/MnO_2 hydrogels. On the other hand, PEDOT/Alg and PEDOT/Alg/CNP hydrogels were used in subsequent characterization studies for comparison purposes.

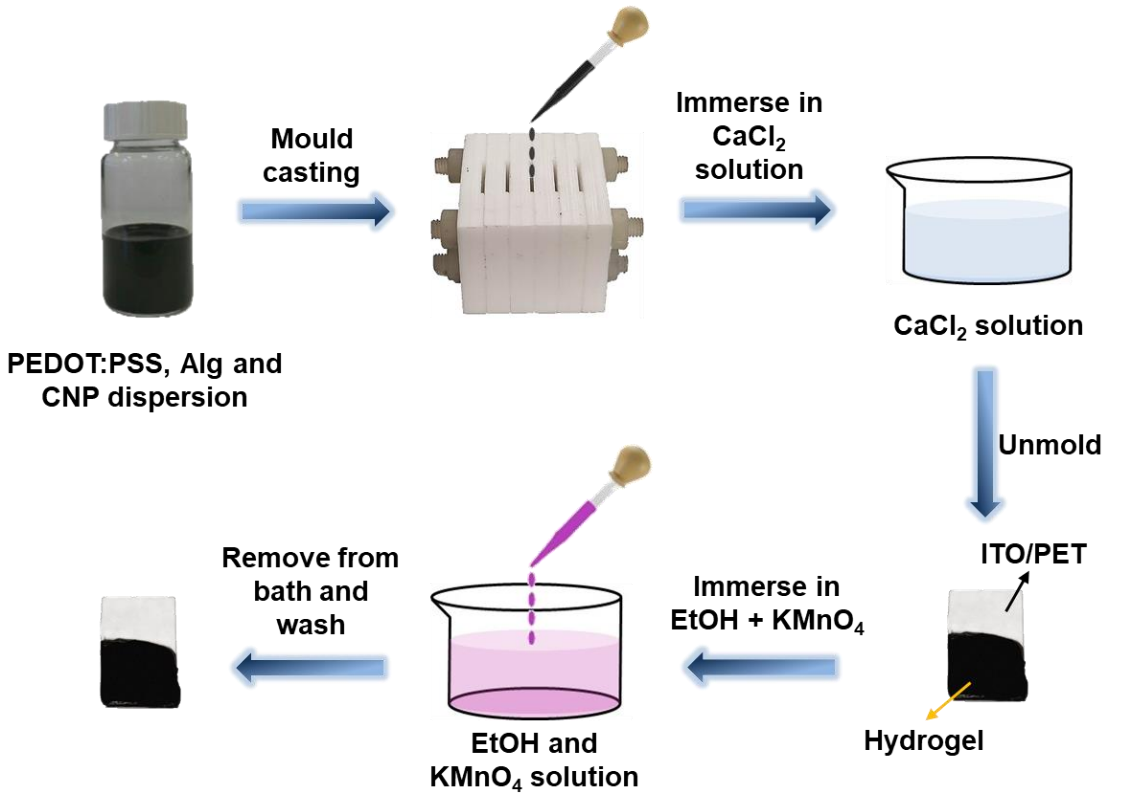

Figure 1. Scheme showing the preparation procedure of the PEDOT/Alg/CNP/MnO_2 hydrogels. Photographs of the prepared hydrogel before and after the incorporation of MnO_2 are shown.

Morphological and spectroscopic analysis.

Figure 2A compares SEM images of the surface of PEDOT/Alg, PEDOT/Alg/CNP and PEDOT/Alg/CNP/MnO_2 hydrogels after lyophilisation. Although all hydrogels exhibit open and interconnected porous structures, these are more evident in PEDOT/Alg than in the CNP and CNP/MnO_2-containing hydrogels (inset in Figure 2A-a1). These features represent an advantage since a high surface area is expected allowing an easy access and a rapid motion of the electrolyte to the hydrogel surface, favouring charge-discharge processes (*i.e.* high energy storage capability). On the other hand, Figure 2A-a2 evidences that the CNP detected in PEDOT/Alg/CNP are homogeneously distributed. Finally, the incorporation of MnO_2 leads to a drastic change in the surface morphology. Thus, PEDOT/Alg/CNP/MnO_2 hydrogel exhibits a rough surface composed of aggregated round nanostructures.

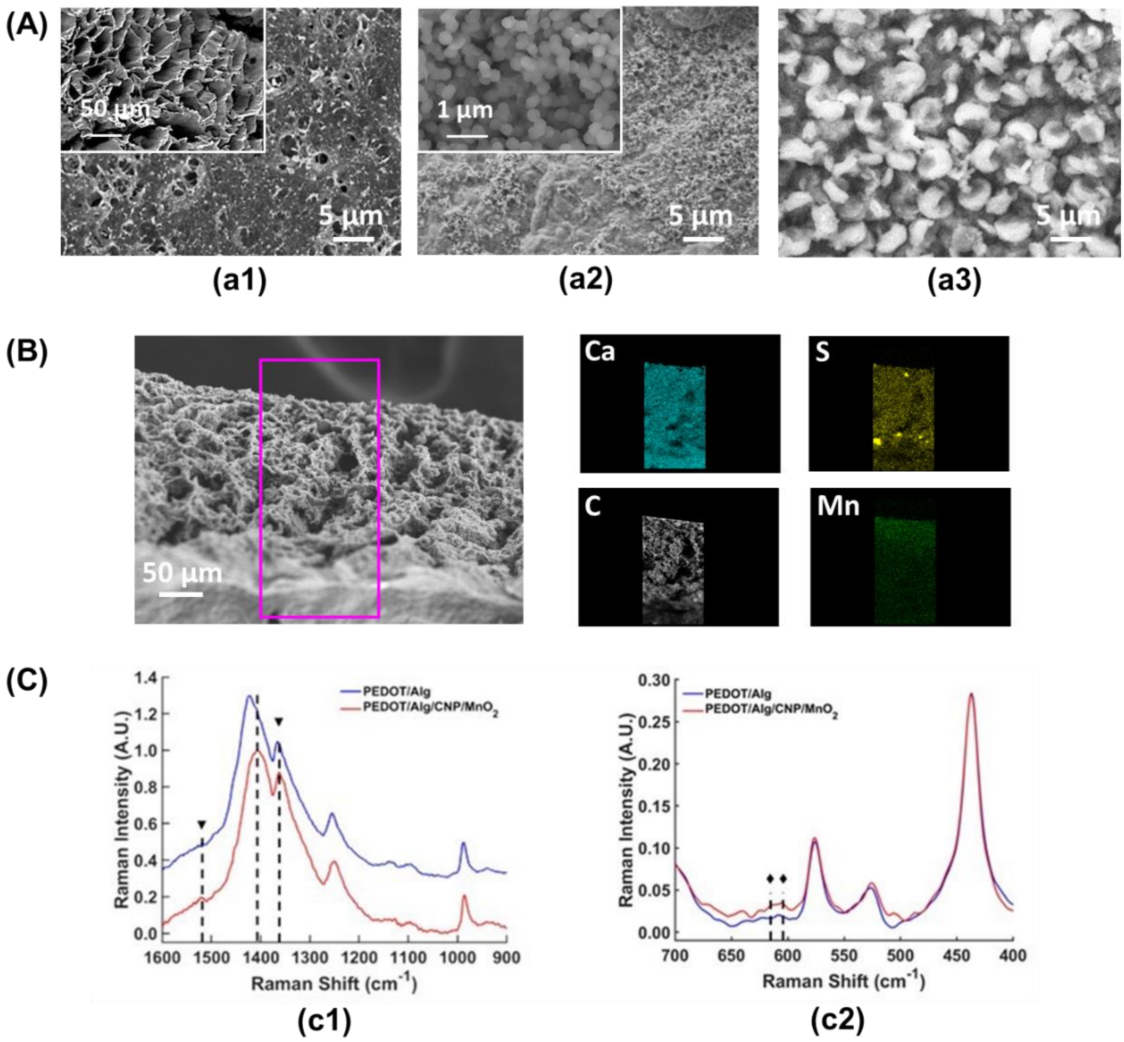

Figure 2. (A) SEM images of (a1) PEDOT/Alg, (a2) PEDOT/Alg/CNP and (a3) PEDOT/Alg/CNP/MnO_2. (B) SEM image and EDX mapping of a PEDOT/Alg/CNP/MnO_2 hydrogel cross-section. (C) Raman spectra of PEDOT/Alg and PEDOT/Alg/CNP/MnO_2 hydrogels.

EDX mapping (Figure 2B) allowed detecting the homogenous distribution of PEDOT and Alg since the S and Ca signals, which are characteristic elements of PEDOT and Alg respectively, are equally detected through the hydrogel. In addition, EDX mapping of the element carbon is detected from the CNP, PEDOT and Alg. Such homogeneous distribution implies that the whole hydrogel is electrically conductive. Finally, the presence of Mn was proven to be not only on the surface but also inside the hydrogel, as the cross-section EDX mapping shows. The latter result confirms the porous and interconnected structure of the hydrogels since the diffusion of EtOH and $KMnO_4$ inside the polymeric network had to take place.

The FTIR spectrum of PEDOT/Alg (Figure S1) is consistent with that already reported for such hydrogel.[23] In addition of the broad band at 3360 cm^{-1}, which is associated to the O–H stretching, the spectrum of PEDOT/Alg displays absorption bands assigned to carbonyl (C=O) asymmetric and symmetric stretching of Alg at 1606 and 1418 cm^{-1}, respectively, the vibrations of the fused dioxane ring from PEDOT at 1286 and 1164 cm^{-1}, the C–O–C stretching of Alg at 1023 cm^{-1}, and the stretch of the C–S bond in the thiophene ring of PEDOT at 822 cm^{-1}. Unfortunately, the spectrum of PEDOT/Alg/CNP does not show any clear evidence of the CNPs (Figure S1), while the PEDOT/Alg/CNP/MnO_2 recorded for samples with the highest MnO_2 content (60 min in the reaction medium) evidences the disappearance of the less intense bands from PEDOT/Alg (Figure S1). This phenomenon has been attributed to the coating effect of MnO_2, which was confirmed by recording the spectra of PEDOT/Alg/CNP/MnO_2 prepared using different MnO_2 content (5, 15, 30 and 60 min in the reaction medium; Figure S2).

Figure 2C shows the Raman spectra of PEDOT/Alg as compared with PEDOT/Alg/CNP/MnO_2. The characteristic bands of PEDOT:PSS can be observed at

1200 – 1500 cm^{-1} (c1).[29] Detection of the rest of components (such as Alg) becomes very difficult as most of the characteristic vibrations are overlapped by the PEDOT signal, which in turn is enhanced by a resonance effect.[30] Nonetheless, the presence of CNP can be observed at 1363 and 1520 cm^{-1}, corresponding to the disorder (D-band) and the tangential mode vibration (G-band) of CNP, respectively.[23] Moreover, the widening and shifting of the PEDOT bands have been attributed to the strong background signal observed in CNP spectra.

On the other hand, several peaks have been detected in the region where manganese oxides are expected (400-900 cm^{-1}). However, the lower intensity of the former peaks compared to PEDOT:PSS and CNP ones make difficult their interpretation (c2). Thus, Raman spectroscopy was run onto the MnO_2 solid obtained after reacting EtOH and $KMnO_4$ without the presence of the hydrogel (Figure S3). Upon closer examination of the manganese oxide region, a sharp peak at 655 cm^{-1}, attributed to the stretching mode of MnO_6 octahedra, is observed along with some weaker peaks in the 400-620 cm^{-1} range. This peak distribution has been assigned to γ-MnO_2 in agreement with the results reported in the literature.[14,17,31,32] Thus, Raman spectra indicates that no significant other manganese species with characteristic Raman fingerprints, like MnOOH or ε-MnO_2,[33,34] are present.

Figure 3 shows the X-ray diffraction (XRD) pattern of the composite hydrogels exhibiting peaks at 2θ values of 25, 37, 55 and 65º assigned to the (120), (021), (221), and (002) planes of γ-MnO_2, as previously reported.[14,17,35] The broad peaks at 25º, 29º and 46º can be ascribed to CNP. These results are in agreement with those previously shown for Raman analysis. It is also worthy to remark that no impurities (*e.g.* $Ca(OH)_2$) are detected in the composite hydrogels.

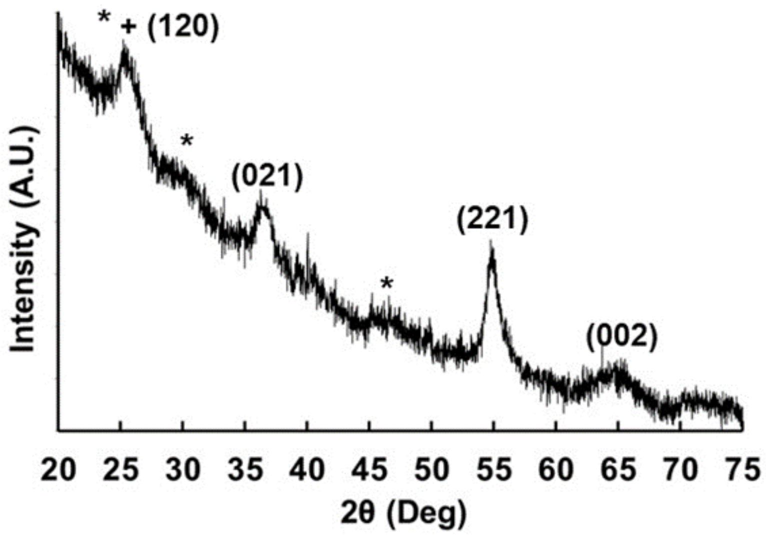

Figure 3. XRD pattern of PEDOT/Alg/CNP/MnO_2. The peaks associated to γ-MnO_2 are indicated. The peaks marked with a star have been ascribed to CNP.

Further morphologic and crystallographic characterization studies using High Resolution Transmission Electron Microscopy (HRTEM) were also performed for the PEDOT/Alg/CNP/MnO_2 multifunctional platform. Figure 4A-B detail the amorphous nature of CNPs illustrated by its twisted fringes, meanwhile in Figure 4C direct observation of the MnO_2 NPs allowed to quantify their average size as 3.76 ± 1.40 nm. Moreover, close inspection of the MnO_2 NPs lattice fringes confirmed that the γ-MnO_2 phase is the predominant, confirming Raman and XRD results. Thus, as it can be observed in the Fast Fourier Transform (FFT) of Figure 4D, detection of the 2.01 Å (120) and 2.13 Å (121) crystallographic planes was attributed to the intergrowth pyrolusite (β-MnO_2) and ramsdellite (ram-MnO_2) structures respectively, confirming the presence of γ-MnO_2. In addition, low presence sole ram-MnO_2 NPs observation (lattice fringe 2.50 Å (021) from Figure 4F) would also be in accordance to the broad peak observed for the (021) reflection in XRD studies due to combination of γ-MnO_2 and ram-MnO_2 NPs.

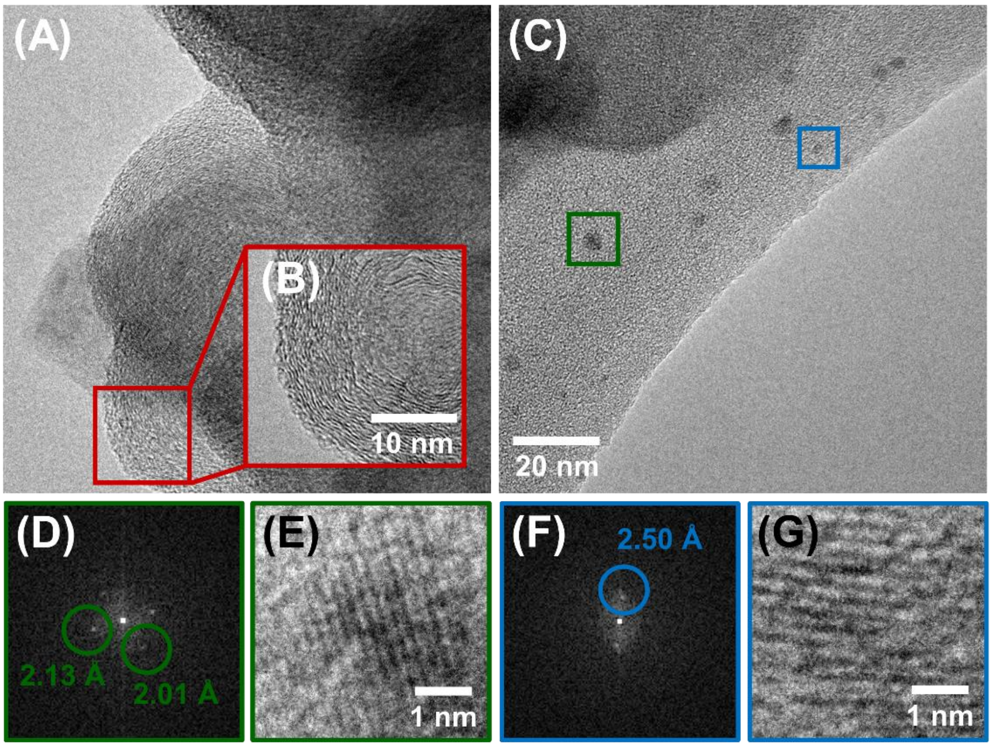

Figure 4. HRTEM images of the PEDOT/Alg/CNP/MnO_2 system. (A) and (B) CNP attached to the PEDOT/Alg structure. (C) Full shot of the PEDOT/Alg/CNP/MnO_2 where the γ-MnO_2 NPs can be appreciated. (D) and (E) Fast Fourier Transform and crystallographic planes for a γ-MnO_2 NP. (F) and (G) Fast Fourier Transform and crystallographic planes for a ram-MnO_2 NP.

The mechanical properties of the prepared hydrogels were evaluated by quantitative nanomechanical AFM mapping. Table 1 lists the Young modulus (E) and the reduced Young modulus (E^*), which are both related by the samples Poisson ratio (ν; Eq 2), of PEDOT/Alg, PEDOT/Alg/CNP and PEDOT/Alg/CNP/MnO_2, considering different permanganate reduction times (t = 5, 15, 30 and 60 min) According to the literature,[36] the value ν was estimated to be 0.5.

$$E^* = \frac{E}{(1-\nu^2)} \qquad (2)$$

The E values were obtained from the force-distance curves (representative examples of the recorded curves are provided in Figure S4). Spin-coated TPU films were examined using a cantilever with a nominal spring constant, k_s, of 5 N/m, with the set point adjusted to get a sample deformation of around 50 nm. As is shown in Table 1, the E value of PEDOT/Alg, ~0.3 MPa, experienced a slight increment to ~0.4 MPa upon the incorporation of CNP. However, the incorporation of MnO_2 to PEDOT/Alg/CNP resulted in a more drastic enlargement of E, which indeed increased with the permanganate reduction time (*i.e.* from ~1 MPa for t = 5 min to ~2 MPa for t = 60 min).

Table 1. Young modulus (E) and the reduced Young modulus (E^*) for the studied hydrogels as determined by quantitative nanomechanical AFM mapping. Measurements on PEDOT/Alg/CNP/MnO_2 were performed considering permanganate reduction times (t).

Sample	***E* (MPa)**	***E** (MPa)**
PEDOT/Alg	0.32 ± 0.05	0.42 ± 0.07
PEDOT/Alg/CNP	0.44 ± 0.08	0.59 ± 0.11
PEDOT/Alg/CNP/MnO_2 (t= 5 min)	1.06 ± 0.08	1.41 ± 0.09
PEDOT/Alg/CNP/MnO_2 (t= 15 min)	0.99 ± 0.18	1.31 ± 0.24
PEDOT/Alg/CNP/MnO_2 (t= 30 min)	1.17 ± 0.31	1.57 ± 0.42
PEDOT/Alg/CNP/MnO_2 (t= 60 min)	1.83 ± 0.56	2.31 ± 0.65

Applications: Supercapacitor and temperature sensing

Initially, cyclic voltammetry (CV) was used to qualitatively characterize the capacitance of the different hydrogels, as the integral area of voltammetric curves is proportional to specific capacitance (Figure 5A). As it can be seen, the presence of CNP increases the capacitance due to the higher electrical conductivity of the hydrogels as well as the energy storage capacity of carbon nanomaterials. However, the incorporation of MnO_2 along with CNP and PEDOT markedly enhances the capacitance of the hydrogels that have been attributed to the following two reasons: (1) the high energy storage capacity of the transition metal oxide; and (2) the low electrical conductivity of MnO_2 is minimized by the presence of CNP and PEDOT, which confer a synergistic behaviour with the inorganic oxide and, therefore, improve its performance.

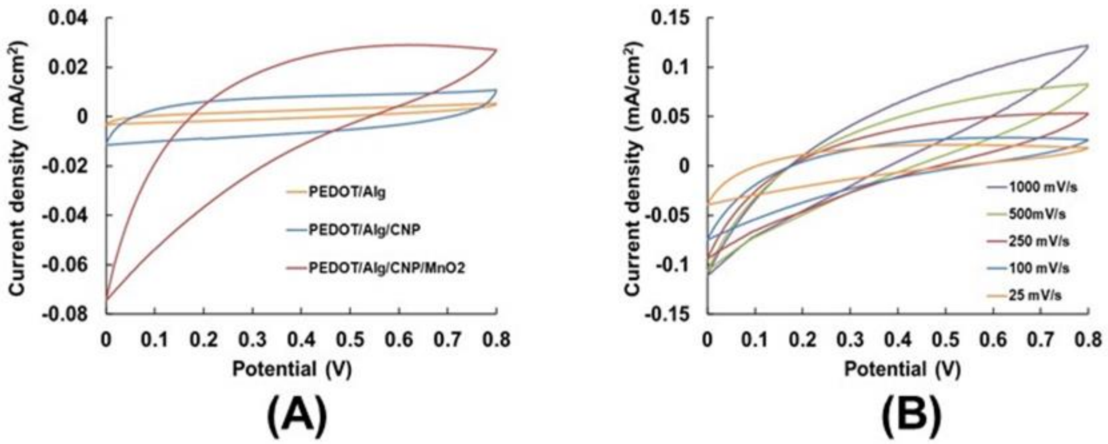

Figure 5. (A) Cyclic voltammograms of PEDOT/Alg, PEDOT/Alg/CNP and PEDOT/Alg/CNP/MnO_2 (t = 30 min) hydrogels at 100 $mV \cdot s^{-1}$. (B) Cyclic voltammograms of PEDOT/Alg/CNP/MnO_2 (t = 30 min) hydrogel at different scan rates.

Cyclic voltammograms of PEDOT/Alg/CNP/MnO_2 hydrogels are characterized by being non-rectangular and symmetric, without redox peaks attributed to the presence of pseudocapacitive materials (e.g. PEDOT, MnO_2), and the good reversibility of the adsorption/desorption and faradaic processes (Figure 5B).[14] On the other hand, the CVs deviate from ideal voltammetric curves (perfectly horizontal) when the scan rate increases from 25 to 1000 $mV \cdot s^{-1}$. Since the energy storage depends on the electrolyte entry / exit into / from the hydrogel (*i.e.* a diffusion-controlled process) and the diffusion of ions is a limited process, the higher the scan rate is, the lower the number of ions that successfully approach and interact with the hydrogel. Good reversibility of the energy storage processes is kept, even at the higher scan rates, as all the curves are symmetric independently of the scan rate.[34] It should be mentioned that capacitive advantages provided by the incorporation of MnO_2 were independent of voltage window. This is illustrated in Figure S5 that compares cyclic voltammogram recorded for PEDOT/Alg/CNP/MnO_2, PEDOT/Alg and PEDOT/Alg/CNP using a potential window from –0.2 V (initial/final potential) to 0.6 V (reversal potential). Also, Figure S5 includes the voltammetric response of PEDOT/Alg/MnO_2 (*i.e.* without CNP) that, as expected, displays a behavior that is intermediate between those of PEDOT/Alg/CNP and PEDOT/Alg/CNP/MnO_2, proving the synergy between MnO_2 and CNP.

The electrochemical stability of PEDOT/Alg, PEDOT/Alg/CNP and PEDOT/Alg/CNP/MnO_2 hydrogels was studied by CV, applying 3000 consecutive redox cycles scanning reversibly a potential window comprised between 0.0 and 0.8 V at a rate of 100 mV/s. Figure 6 compares the evolution of the electroactivity with respect to the second cycle against the number of CV cycles (Eq S1). The stability of PEDOT/Alg was relatively poor, the loss of electroactivity stabilizing at around 71% after 2500 CV cycles. The incorporation of CNP improved the electrochemical performance, the loss of electroactivity reaching a constant value of ~40% after 2000 CV cycles. This improvement was attributed to the intrinsic structural stability of CNP in comparison with neat organic polymers (*i.e.* PEDOT and Alg), which underwent the electrically induced chemical degradation very rapidly. Moreover, such stabilization is much more pronounced for PEDOT/Alg/CNP/MnO_2 due to the intrinsic stability of MnO_2, a crystalline ceramic material. For PEDOT/Alg/CNP/MnO_2, the loss of electroactivity with respect to the second cycle, which was of ~20% only, stabilized after 300 cycles.

To assess the effect of flexibility on the electrochemical response of PEDOT/Alg/CNP/MnO_2, cyclic voltammograms were recorded for the as prepared hydrogel, the bent hydrogel (*i.e.* the hydrogel was completely folded on itself, as is shown in the inset of Figure S6), and after such drastic bending. Results, shown in Figure S6, indicate that although the electrochemical activity decreased under folding due to percolation loss of both CNP and MnO_2 when the hydrogel is under bending forces, the electrochemical activity largely recovers when the hydrogel comes back to the original state (after bending). Consistently, the energy density before and after the bending were very similar ($1.05 \cdot 10^{-4}$ and $1.09 \cdot 10^{-4}$ J/m^3, respectively), while the energy density of the bent sample was much lower ($5.34 \cdot 10^{-5}$ J/m^3).

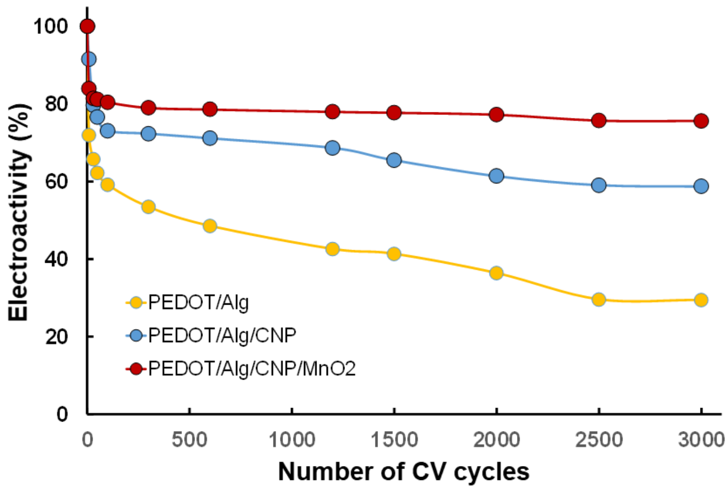

Figure 6. Variation of the electroactivity (with respect to the second cycle) against the number of CV cycles (Eq S1).

The effect of CNPs and MnO_2 on the electrical resistance (R) of PEDOT/Alg was examined by electrochemical chemical impedance (EIS) spectroscopy measurements. The resistance was obtained adjusting the recorded Nyquist plots, which are shown in Figure S7, to a simple Randless circuit. Results show that the electrical resistance of PEDOT/Alg experiences a slight reduction upon the incorporation of CNPs (R = 15.8 and 14.6 kΩ·cm^{-2} for PEDOT/Alg and PEDOT/Alg/CNP, respectively). Besides, the resistance of MnO_2-containing system is lower by one order of magnitude (R = 3.4 kΩ·cm^{-2} for PEDOT/Alg/CNP/MnO_2), which is fully consistent with its enhanced electrochemical behavior.

After that, the performance of PEDOT/Alg/CNP/MnO_2 hydrogels prepared with different MnO_2 content was quantitatively evaluated using GCD assays (Figure 7A). The area of the GCD curves and, therefore, the capacitance (Eq S2) rapidly increased with the permanganate reduction time, until a threshold value of 30 min was reached (Figure 7B).

Thus, the capacitance of PEDO/Alg/CNP, which was 6 ± 1 mF cm^{-2} (t = 0 min), increased to 9 ± 1 mF cm^{-2} after the shortest time in the permanganate reduction medium (t = 5 min), reaching a value of 42 ± 2 mF cm^{-2} when the time in the medium increased to 30 min (Figure 7B). Although this value is higher than values reported for many multi-component soft materials used in wearable supercapacitors, as for example PEDOT/reduced graphene oxide hydrogel (25 mF cm^{-2})[37] polyaniline/carbon nanotubes (PANI/CNT) yarn (38 mF cm^{-2})[38] and graphene textile (2.7 mF·cm^{-2}),[39] some single component electroactive materials have exhibited greater values, as for example air stable PANI ink (96 mF·cm^{-2}).[40] Beyond 30 min, the capacitance decreased to 19 ± 3 mF cm^{-2} (Figure 7B) due to the higher content of MnO_2 and, therefore, the lower electrical conductivity of the hydrogel. On the other hand, the GCD curves systematically deviate from the ideal triangular curves (Figure 7C) due to the pseudocapacitive materials, in agreement with the results found by CV. Despite the slight asymmetry in the GCD curves, the coulombic efficiency (η; Eq 1), which corresponds to the ratio between the charge (t_c) and discharge times (t_d), is very good (87±3 %).

$$\eta = \frac{t_c}{t_d} \qquad (1)$$

On the other hand, no voltage drop is observed in the GCD curves, indicating that the internal resistance of the hydrogels is low due to the continuous electrical path created by CNP and PEDOT. Finally, life cycle was evaluated by performing 3000 consecutive GCD cycles. Around 80% of the initial capacitance was retained after such huge amount of cycles (Figure 7), indicating a good rate capability of the hydrogels.

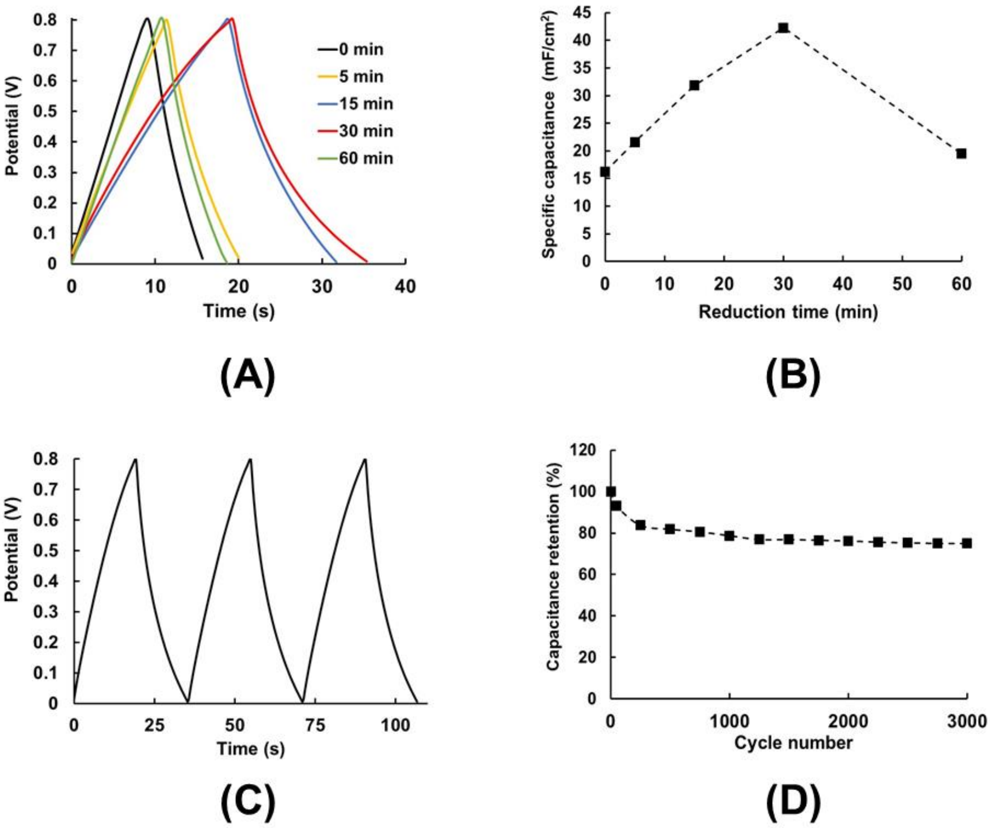

Figure 7. (A) GCD curves of PEDOT/Alg/CNP/MnO_2 prepared using different permanganate reduction times. (B) Variation of the specific capacitance of PEDOT/Alg/CNP/MnO_2 against the permanganate reduction time. (C) Consecutive GCD curves of PEDOT/Alg/CNP/MnO_2 prepared using a permanganate reduction time of 30 min. (D) Life cycle stability for 3000 GCD cycles.

The electrochemical performance of two PEDOT/Alg/CNP/MnO_2 supercapacitors connected in parallel and series modes was also examined. In both cases an Alg hydrogel was used as semi-solid dielectric medium. The recorded voltammograms are shown in Figure 8A, while Figure 8B sketches the connections between the different components for the two studied modes (photographs are displayed in Figure S8). While a vanishing effect is observed when the supercapactior were connected in series, the current density and, therefore, the voltammetric area increased significantly for the parallel mode. This confirms the good behavior of PEDOT/Alg/CNP/MnO_2 as supercapacitors.

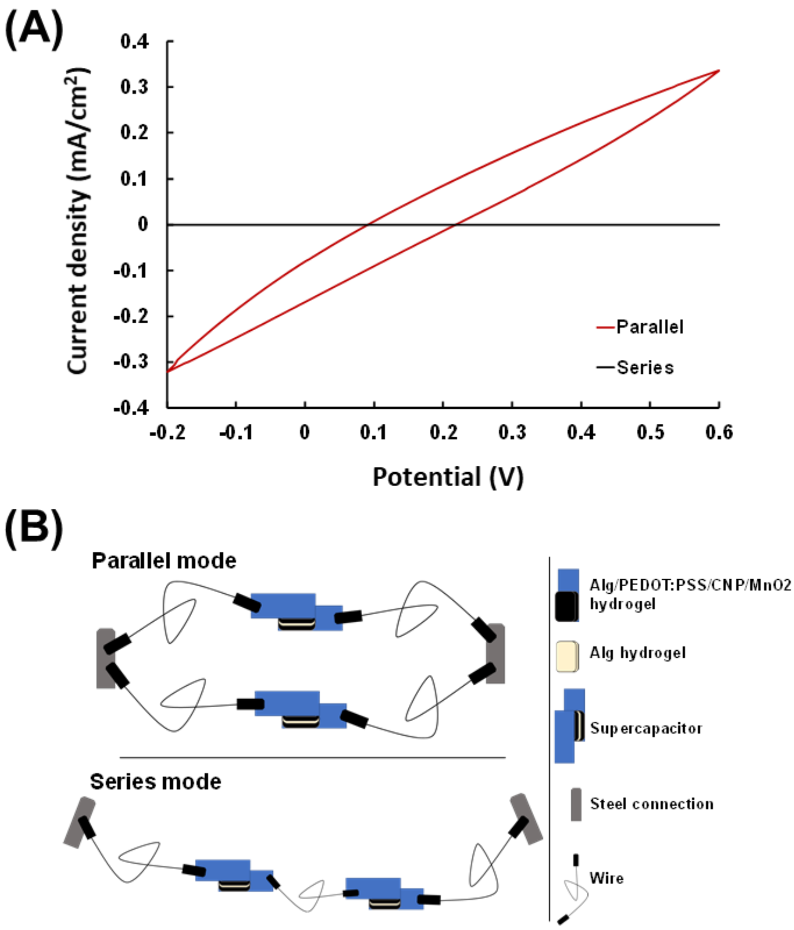

Figure 8. (A) Voltammograms recorded for two PEDOT/Alg/CNP/MnO_2 supercapacitors connected in series and parallel (Alg hydrogel was used as semi-solid dielectric medium). (B) Diagram showing the connections between the different components for the supercapacitors connected in series and parallel modes.

PEDOT/Alg/CNP/MnO_2 hydrogels were studied to be simultaneously used as temperature sensor. The normalized resistance ($\Delta R/R_0$) was measured when the temperature was increased from 20 to 60 ºC considering the two orthogonal directions (Figure 9A-B). As it can be observed, the sensing capacity of the hydrogel is independent of the measurement direction. The electrical conductivity of the hydrogel increases with the temperature, leading to a decrease in the normalized resistance. This is because PEDOT and carbon nanomaterials are semiconducting materials and, therefore, their conductivity increases as temperature rises due to the higher number of charge carriers.[41,42] Indeed, the linear decrease of the normalized resistance is fully consistent with the semiconducting behaviour exhibited by materials with a positive temperature coefficient, such as PEDOT:PSS.[43] Thus, the charge transport regime in PEDOT/Alg/CNP/MnO_2 hydrogels is thermally activated. After cooling, the same $\Delta R/R_0$ values were practically obtained while no hysteresis was detected, indicating good reproducibility of the sensor. This feature has been attributed to the fact that no water removal occurs in the temperature interval comprised between 25 to 60 ºC, which could alter the chemical composition of the system and/or the mechanical consistency of the hydrogel. On the other hand, the sensitivity of the hydrogel was evaluated through the temperature coefficient of resistance (TCR) calculated as follows (Eq 3):

$$TCR = \frac{R-R_0}{R_0} \cdot \frac{1}{\Delta T} \cdot 100 \qquad (3)$$

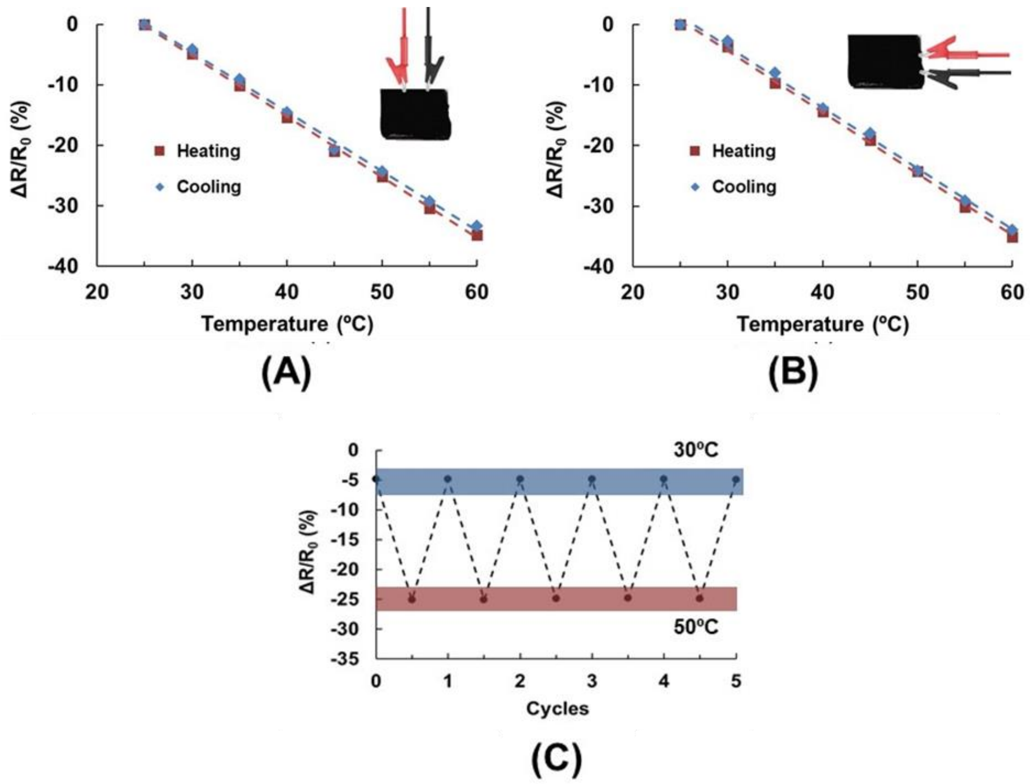

Figure 9. For PEDOT/Alg/CNP/MnO_2 prepared using a permanganate reduction time of 30 min: (A, B) Variation of the normalized resistance with temperature during heating and cooling in the two directions of the sample; and (C) Normalized resistance after different heating/cooling cycles.

The sensitivity is -1.05 ± 0.10 % $°C^{-1}$, which is significantly higher than the values reported for other materials based on PEDOT and carbon nanomaterials.[41,42,44,45] For example, inkjet-printed samples based on carbon and PEDOT:PSS and screen-printed samples PEDOT:PSS/CNTs reached a TCR of 0.25 and 0.61 % $°C^{-1}$, respectively.[43,44] Also other CPs, such as polyaniline nanofibers, have been used to fabricate temperature sensors. For example, the TCR reported for PANI electrochemically polymerized on a polyethylene terephthalate sheet was 0.61 % $°C^{-1}$.[45] It is important to highlight that the presence of MnO_2 do not hinder the variation of resistance with temperature. Finally, the hydrogel was reproducible as similar values were obtained after a few heating/cooling cycles (Figure 9C).

Therefore, a new strategy to develop multifunctional composite hydrogels for energy storage and temperature sensing has been designed. This is based on: (i) using hydrogels with open and interconnected porosity to improve electrolyte access; (ii) incorporating CNP and PEDOT to confer electrical conductivity for temperature sensing and create effective electron pathways; and (iii) adding MnO_2 to improve the energy storage capacity of the hydrogel.

CONCLUSIONS

In summary, multifunctional PEDOT/Alg/CNP/MnO_2 hydrogels for supercapacitors and temperature sensors have successfully fabricated. For this purpose, initially PEDOT/Alg/CNP hydrogels were prepared by casting molding. Next, a chemical reduction process of permanganate to MnO_2 was applied to obtain PEDOT/Alg/CNP/MnO_2. The specific capacitance increased due to the presence of CNP as well as the incorporation of MnO_2, which is a highly capacitive material. The composite hydrogel shows good capacitance values (42 mF/cm^2) and good long term cyclability (87 %) probably due to both: 1) the presence of MnO_2 into the electrically conductive CNP and PEDOT matrix; and 2) the open and interconnected structure of the hydrogels that facilitates the adsorption/desorption or faradaic processes. Finally, the PEDOT/Alg/CNP/MnO_2 hydrogels can be successfully used to sense temperature by measuring changes in the normalized resistance, showing an excellent coefficient of temperature (-1.05 % $°C^{-1}$). Overall, PEDOT/Alg/CNP/MnO_2 hydrogels are promising for applications in multifunctional flexible and wearable electronics.

ASSOCIATED CONTENT

The Supporting Information is available free of charge at https://pubs.acs.org/doi/

Materials and characterization methods, FTIR and Raman spectra, representative force-distance curves determined by quantitative nanomechanical AFM mapping, cyclic voltammograms, Nyquist plots, and photograps of two supercapacitors connected in parallel and series modes.

CONFLICTS OF INTERESTS

The authors declare that they have no known competing financial interests or personal relationships that could have appeared to influence the work reported in this paper.

ACKNOWLEDGEMENTS

Authors acknowledge the grants RTI2018-098951-B-I00, PID2019-103892RB-I00 and PLEC2022-009279 funded by MCIN/AEI/10.13039/501100011033 and the support of the Agència de Gestió d'Ajuts Universitaris i de Recerca (2021 SGR 00387, 2021 SGR

01368). Support for the research of C.A. and M.-P.G. was also received through the prize “ICREA Academia” for excellence in research funded by the Generalitat de Catalunya. J.G.-T. acknowledges the Serra Hunter program of the Generalitat de Catalunya.

REFERENCES

1. Dechiraju, H.; Jia, M. P.; Luo, L.; Rolandi, M. On-Conducting Hydrogels and Their Applications in Bioelectronics. *Adv. Sustain. Syst.* **2021**, *6*, 2100173.
2. Hao, X. P.; Li, C. Y.; Zhang, C. W.; Du, M.; Ying, Z. M.; Zheng, Q.; Wu, Z. L. Self-Shaping Soft Electronics Based on Patterned Hydrogel with Stencil-Printed Liquid Metal. *Adv. Funct. Mater.* **2021**, *31*, 2105481.
3. Alamdari, S. G.; Alibakhshi, A.; de la Guardia, M.; Baradaran, R.; Mohammadzadeh, R.; Amini, M.; Kesharwani, P.; Mokhtardadeh, A.; Oroojalian, F.; Sahebkar, A. Conductive and Semiconductive Nanocomposite-Based Hydrogels for Cardiac Tissue Engineering. *Adv. Healthc. Mater.* **2022**, *11*, 2200526.
4. Sun, J.-Y.; Zhao, X.; Illeperuma, W. R. K.; Chaudhuri, O.; Oh, K. H.; Mooney, D. J.; Vlassaki, J. J.; Suo, Z. Highly Stretchable and Tough Hydrogels. *Nature* **2012**, *489*, 133–136.
5. Ren, X.; Yang, M.; Yang, T.; Xu, C.; Ye, Y.; Wu, X.; Zheng, X.; Wang, B.; Wan, Y.; Luo, Z. Highly Conductive PPy–PEDOT:PSS Hybrid Hydrogel with Superior Biocompatibility for Bioelectronics Application. *ACS Appl. Mater. Interfaces* **2021**, *13*, 25374–25382.
6. Zhang, S.; Chen, Y.; Liu, H.; Wang, Z.; Ling, H.; Wang, C.; Ni, J.; Saltik, B. C.; Wang, X.; Meng, X.; Kim, H.-J.; Baidya, A.; Ahadian, S.; Ashammakhi, N.; Dokmeci, M. R.; Travas-Sejdic, J.; Khademhosseini, A. Room-Temperature-Formed

PEDOT:PSS Hydrogels Enable Injectable, Soft, and Healable Organic Bioelectronics. *Adv. Mater.* **2020**, *32*, 1904752.

7. Jiang, G.; Wang, G.; Zhu, Y.; Cheng, W.; Cao, K.; Xu, G.; Zhao, D.; Yu, H. A Scalable Bacterial Cellulose Ionogel for Multisensory Electronic Skin. *Research* **2022**, *2022*, 9814767.
8. Cheng, W.; Liu, Y.; Tongi, Z.; Zhu, Y.; Cao, K.; Chen, W.; Zhao, D.; Yu, H. Micro-Interfacial Polymerization of Porous PEDOT for Printable Electronic Devices. *EcoMat*. **2023**, *5*, e12288.
9. Singh, R.; Veer, B. Hydrogels: Promising Energy Storage Materials. *Chem. Select* **2018**, *3*, 1309–1320.
10. Zhang, W.; Feng, P.; Chen, J.; Sun, Z.; Zhao, B. Electrically conductive hydrogels for flexible energy storage systems. *Progr. Polym. Sci.* **2019**, *88*, 220–240.
11. Zhao, Q.; Liu, J.; Wu, Z.; Xu, X.; Ma, H.; Hou, J.; Xu, Q.; Yang, R.; Zhang, K.; Zhang, M.; Yang, H.; Peng, W. Liu, X.; Zhang, C.; Xu, J.; Lu, B. Robust PEDOT:PSS-Based Hydrogel for Highly Efficient Interfacial Solar Water Purification. *Chem. Eng. J.* **2022**, *442*, 136284.
12. Yang, Y.; Yang, X.; Tan, Y.; Yuan, Q. Recent Progress in Flexible and Wearable Bio-Electronics Based on Nanomaterials. *Nano Res.* **2017**, *10*, 1560–1583.
13. Zhang, Y.; Liang, B.; Jiang, Q.; Li, Y.; Feng, Y.; Zhang, L.; Zhao, Y.; Xiong, X. Flexible and Wearable Sensor Based on Graphene Nanocomposite Hydrogels. *Smart Mater. Struct.* **2020**, *29*, 075027.
14. Garcia-Torres, J.; Crean, C. Ternary Composite Solid-State Flexible Supercapacitor Based on Nanocarbons/Manganese Dioxide/PEDOT:PSS Fibres. *Mater. Design* **2018**, *155*, 194–202.

15. Qin, Z.; Sun, X.; Yu, Q.; Zhang, H.; Wu, X.; Yao, M.; Liu, W.; Yao, F.; Li, J. Carbon Nanotubes/Hydrophobically Associated Hydrogels as Ultrastretchable, Highly Sensitive, Stable Strain, and Pressure Sensors. *ACS Appl. Mater. Interfaces* **2020**, *12*, 4944–4953.

16. Patil, S. J.; Chodankar, N. R.; Han, Y.-K.; Lee, D. W. Carbon Alternative Pseudocapacitive V_2O_5 Nanobricks and δ-MnO_2 Nanoflakes@ α-MnO_2 Nanowires Hetero-Phase for High-Energy Pseudocapacitor. *J. Power Sources* **2020**, *453*, 227766.

17. Garcia-Torres, J.; Crean, C. Multilayered Flexible Fibers with High Performance for Wearable Supercapacitor Applications. *Adv. Sust. Syst.* **2018**, *2*, 1700143.

18. García-Torres, J.; Colombi, S.; Macor, L. P.; Alemán, C. Multitasking Smart Hydrogels Based on the Combination of Alginate and Poly(3,4-ethylenedioxythiophene) Properties: A review. *Int. J. Biol. Macromol.* **2022**, *219*, 312–332.

19. Gueye, M. N.; Carella, A.; Faure-Vincent, J.; Demadrille, R.; Simonato, J. P. Progress in Understanding Structure and Transport Properties of PEDOT-Based Materials: A Critical Review. *Prog. Mater. Sci.* **2020**, *108*, 100616.

20. Sun, K.; Zhang, S.; Li, P.; Xia, Y.; Zhang, X.; Du, D.; Isikgor, F. H.; Ouyang, J. Review on Application of PEDOTs and PEDOT:PSS in Energy Conversion and Storage Devices. *J. Mater. Sci. Mater. Electron.* **2015**, *26*, 4438–4462.

21. Fabregat, G.; Teixeira-Dias, B.; del Valle, L. J.; Armelin, F.; Estrany, F.; Alemán. Incorporation of a Clot-Binding Peptide into Polythiophene: Properties of Composites for Biomedical Applications. *ACS Appl. Mater. Interfaces* **2014**, *6*, 11940–11954

22. Pawar, N.; Edgar, K. J. Alginate Derivatization: A Review of Chemistry, Properties and Applications. *Biomaterials* **2012**, *33*, 3279–3305.
23. Babeli, I.; Ruano, G.; Casanovas, J.; Ginebra, M. P.; García-Torres, J.; Alemán, C. Conductive, Self-Healable and Reusable Poly(3,4-ethylenedioxythiophene)-Based Hydrogels for Highly Sensitive Pressure Arrays. *J. Mater. Chem. C* **2020**, *8*, 8654–8667.
24. Puiggalí-Jou, A.; Cazorla, E.; Ruano, G.; Babeli, I.; Ginebra, M. P.; García-Torres, J.; Alemán, C. Electroresponsive Alginate-Based Hydrogels for Controlled Release of Hydrophobic Drugs. *ACS Biomater. Sci. Eng.* **2020**, *6*, 6228–6240.
25. Paradee, N.; Sirivat, A. Electrically Controlled Release of Benzoic Acid from Poly(3,4-ethylenedioxythiophene)/Alginate Matrix: Effect of Conductive Poly(3,4-ethylenedioxythiophene) Morphology. *J. Phys. Chem. B* **2014**, *118*, 9263–9271.
26. Babeli, I.; Puiggalí-Jou, A.; Roa, J.J.; Ginebra, M. P.; García-Torres, J.; Alemán, C. Hybrid Conducting Alginate-Based Hydrogel for Hydrogen Peroxide Detection from Enzymatic Oxidation of Lactate. *Int. J. Biol. Macromol.* **2021**, *193*, 1237–1248.
27. Puiggalí-Jou, A.; Babeli, I.; Roa, J. J.; Zoppe, J. O.; Garcia-Amorós, J.; Ginebra, M. P.; Alemán, C.; García-Torres, J. Remote Spatiotemporal Control of a Magnetic and Electroconductive Hydrogel Network via Magnetic Fields for Soft Electronic Applications. *ACS Appl. Mater. Interfaces* **2021**, *13*, 42486–42501.
28. Toupin, M.; Brousse, T.; Belanger, D. Charge Storage Mechanism of MnO_2 Electrode Used in Aqueous Electrochemical Capacitor. *Chem. Mater.* **2004**, *16*, 3184–3190.
29. Baddour-Hadjean, R.; Pereira-Ramos, J.-P. Raman Microspectrometry Applied to the Study of Electrode Materials for Lithium Batteries. *Chem. Rev.* **2010**, *110*, 1278–1319.

30. Salvaterra, R. V.; Moura, L. G.; Oliveira, M. M.; Pimienta, M. A.; Zarbin, A. J. G. Resonant Raman Spectroscopy and Spectroelectrochemistry Characterization of Carbon Nanotubes/Polyaniline Thin Film Obtained Through Interfacial Polymerization. *J. Raman Spectrosc.* **2012**, *43*, 1094–1100.

31. Adelkham, H.; Ghaemi, M.; Jafari, S. M. Novel Nanostructured MnO2 Prepared by Pulse Electrodeposition: Characterization and Electrokinetics. *J. Mater. Sci. Technol.* **2008**, *24*, 857–852.

32. Han, G.; Liu, Y.; Zhang, L.; Kan, E.; Zhang, S.; Tang, J.; Tang, W. MnO_2 Nanorods Intercalating Graphene Oxide/Polyaniline Ternary Composites for Robust High-Performance Supercapacitors. Sci. Rep. 2014, 4, 4824.

33. Zhang, Z.; Dang, W.; Dong, C.; Chen, G.; Wang, Y.; Guan, H. Facile Synthesis of Core–Shell Carbon Nanotubes@MnOOH Nanocomposites with Remarkable Dielectric Loss and Electromagnetic Shielding Properties. *RSC Adv*. **2016**, *6*, 90002–90009

34. Garcia-Torres, J.; Roberts, A. J.; Slade, R. C. T.; Crean, C. One-Step Wet-Spinning Process of CB/CNT/MnO_2 Nanotubes Hybrid Flexible Fibres as Electrodes for Wearable Supercapacitors. *Electrochim. Acta* **2019**, *296*, 481–490.

35. Yang, L.; Cheng, S.; Ji, X.; Jiang, Y.; Zhou, J.; Liu, M. Investigations Into the Origin of Pseudocapacitive Behavior of Mn_3O_4 Electrodes using *in operando* Raman spectroscopy. *J. Mater. Chem. A* **2015**, *3*, 7338–7344.

36. Javanmardi, Y.; Colin-York, H.; Szita, N.; Fritzsche, M.; Moeendarbary, E. Quantifying Cell-Generated Forces: Poisson's Ratio Matters. *Commun. Phys* **2021**, *4*, 237.

37. Lehtimäki, S.; Suominen, M.; Dmalin, P.; Tuukkanen, S.; Kvarnström, C.; Lupo, D. Preparation of Supercapacitors on Flexible Substrates with Electrodeposited PEDOT/Graphene Composites. *ACS Appl. Mater. Interfaces* **2015**, *7*, 22137–22147.
38. Wang, K.; Meng, Q.; Zhang, Y.; Wei, Z.; Miao, M. High-Performance Two-Ply Yarn Supercapacitors Based on Carbon Nanotubes and Polyaniline Nanowire Arrays. *Adv. Mater.* **2013**, *25*, 1494–1498.
39. Afroj, S.; Tan, S.; Abdelkader, A. M.; Novoselov, K. S.; Karim, N. Highly Conductive, Scalable, and Machine Washable Graphene-Based E-Textiles for Multifunctional Wearable Electronic Applications. *Adv. Funct. Mater.* **2020**, *30*, 2000293.
40. Chu, X.; Chen, G.; Xiao, X.; Wang, Z.; Yang, T.; Xu, Z.; Huang, H.; Wang, Y.; Yan, C.; Chen, N.; Zhang, H.; Yang, W.; Chen, J.; Air-Stable Conductive Polymer Ink for Printed Wearable Micro-Supercapacitors. *Small* **2021**, *17*, 2100956.
41. Vuorinen, T.; Niittynen, J.; Kankkunen, T.; Kraft, T. M.; Mantysalo, M. Temperature Sensors on a Skin-Conformable Polyurethane Substrate. *Sci. Rep.* **2016**, *6*, 35289.
42. Honda, W.; Harada, S.; Arie, T.; Akita, S.; Takei, K. Wearable, Human-Interactive, Health-Monitoring, Wireless Devices Fabricated by Macroscale Printing Techniques. *Adv. Funct. Mater.* **2014**, *24*, 3299–3304.
43. Zhou, J.; Anjum, D. H.; Chen, L.; Xu, X.; Aguilar Ventura, I.; Jiang, L.; Lubineau, J. The Temperature-Dependent Microstructure of PEDOT/PSS Films: Insights from Morphological, Mechanical and Electrical Analyses. *J. Mater. Chem. C* **2014**, *2*, 9903–9910.
44. Bali, C.; Brandlmaier, A.; Ganster, A.; Raab, O.; Zapf, J.; Hübler, A. Fully Inkjet-Printed Flexible Temperature Sensors Based on Carbon and PEDOT:PSS. *Mater. Today: Proc.* **2016**, *3*, 739–745.

45. Hong, S. Y.; Lee, Y. H.; Park, H.; Jin, S. W.; Jeong, Y. R.; Yun, J.; You, I.; Zi, G.; Ha, J. S. Stretchable Active Matrix Temperature Sensor Array of Polyaniline Nanofibers for Electronic Skin. *Adv. Mater*. **2016**, *28*, 930–935.

Table of Contents

Jose Garcia-Torres, Ikraan Mahamed, Dioulde Sylla, Jordi Sans, Maria-Pau Ginebra, Carlos Alemán**

Multifunctional hydrogels for simultaneous energy storage and temperature sensing